analytical chemistry

Article

Cite This: Anal. Chem. 2018, 90, 11232−11239

pubs.acs.org/ac

# Direct Determination of Aerosol pH: Size-Resolved Measurements of Submicrometer and Supermicrometer Aqueous Particles

Rebecca L. Craig,[†] Peter K. Peterson,[†] Lucy Nandy,[§] Ziying Lei,[‡] Mohammed A. Hossain,[†] Stephanie Camarena,[†] Ryan A. Dodson,[†] Ryan D. Cook,[†] Cari S. Dutcher,[§] and Andrew P. Ault*[,†,‡]

[†]Department of Chemistry, and [‡]Department of Environmental Health Sciences, University of Michigan, Ann Arbor, Michigan 48109, United States

[§]Department of Mechanical Engineering, University of Minnesota, Minneapolis, Minnesota 55455, United States

Supporting Information

**ABSTRACT:** Measuring the acidity of atmospheric aerosols is critical, as many key multiphase chemical reactions involving aerosols are highly pH-dependent. These reactions impact processes, such as secondary organic aerosol (SOA) formation, that impact climate and health. However, determining the pH of atmospheric particles, which have minute volumes ($10^{-23}$−$10^{-18}$ L), is an analytical challenge due to the nonconservative nature of the hydronium ion, particularly as most chemical aerosol measurements are made offline or under vacuum, where water can be lost and acid−base equilibria shifted. Because of these challenges, there have been no direct methods to probe atmospheric aerosol acidity, and pH has typically been determined by proxy/indirect methods, such as ion balance, or thermodynamic models. Herein, we present a novel and facile method for direct measurement of size-resolved aerosol acidity from pH 0 to 4.5 using quantitative colorimetric image processing of cellular phone images of $(NH_4)_2SO_4$−$H_2SO_4$ aqueous aerosol particles impacted onto pH-indicator paper. A trend of increasing aerosol acidity with decreasing particle size was observed that is consistent with spectroscopic measurements of individual particle pH. These results indicate the potential for direct measurements of size-resolved atmospheric aerosol acidity, which is needed to improve fundamental understanding of pH-dependent atmospheric processes, such as SOA formation.

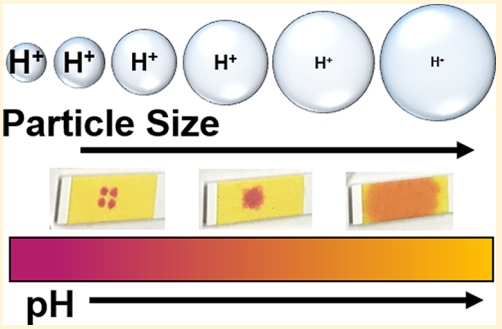


Atmospheric aerosols have global impacts on human health (10% of global deaths annually)[1] and climate (due to effects on radiative forcing and cloud formation).[2] Despite their importance, mechanistic understanding is low for many key atmospheric processes, such as secondary organic aerosol (SOA) formation. Aerosol acidity is a critical property for SOA formation, specifically epoxide ring-opening reactions, as the reaction rates of pH-dependent multiphase chemical processes can vary by 5 orders of magnitude within relevant atmospheric pH values (0−5), leading to lifetimes for key species that vary from minutes to weeks.[3,4] Other multiphase chemical processes where acidic pH conditions are important include gas−aerosol phase partitioning,[3] heterogeneous reactions,[5−7] water uptake,[8,9] hydrolysis,[10−12] liquid−liquid phase separations,[13−15] metal ion dissolution and solubility,[16−19] and photolysis and OH reaction chemistry.[20,21] Recent work has predicted through indirect methods that aerosol particles are often acidic,[22−26] which is important for the processes listed above. In addition to a lack of direct measurements, there is uncertainty regarding atmospheric aerosol acidity due to differing source contributions,[27,28] seasonality,[29,30] and location (urban vs rural).[25]

Aerosol acidity is difficult to measure due to the nonconservative nature of $H^+$ concentration and its dependence on solvent concentration, which is determined by relative humidity (RH) and aerosol liquid water content. As such, filter-based measurements or proxy methods that do not measure water when predicting pH are often used. Filter-based methods involve extraction with solvents that can shift the equilibria of ions present, leading to high uncertainties. Proxy methods include ion balance, molar ratio, phase partitioning, and thermodynamic equilibrium models, with the latter two regarded as the most accurate.[31,32] For the phase partitioning method, gas and aerosol phase measurements of semivolatile compounds, such as $NH_3/NH_4^+$, are used to indirectly measure pH.[31,33] Thermodynamic models, such as E-AIM[34−36] and ISORROPIA-II,[37,38] predict aerosol pH based on measured chemical species (e.g., sulfate and ammonium concentrations), temperature, and RH and have been increasingly applied to evaluate atmospheric aerosol acidity and variability.[22−26,28,29] Given the lack of approaches to directly measure pH, these models have driven our knowledge of aerosol acidity, but have also had few experimental measurements of pH to constrain their results. In particular, the thermodynamic models are most accurate when they can be constrained by measurements of both gas and particle phase

Received: February 4, 2018
Accepted: August 28, 2018
Published: September 11, 2018






DOI: 10.1021/acs.analchem.8b00586
Anal. Chem. 2018, 90, 11232−11239

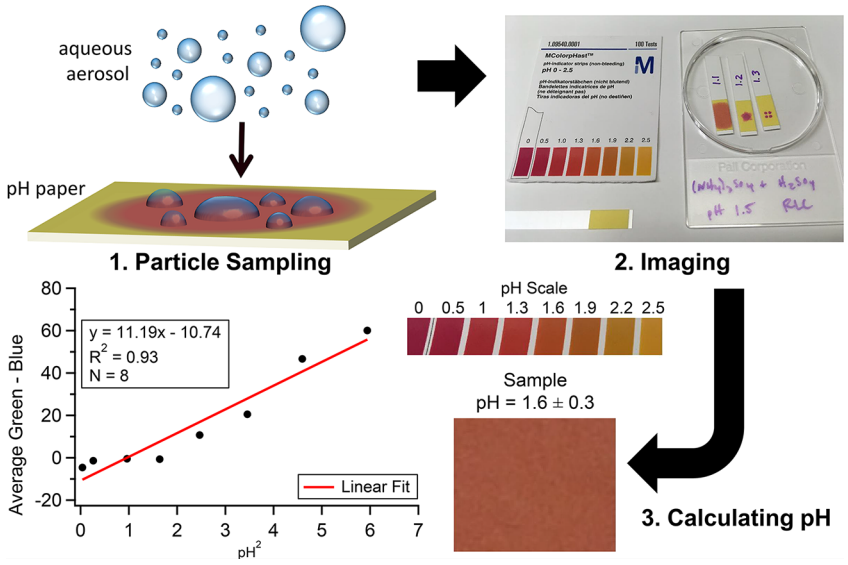


**Figure 1.** Schematic of pH indicator paper method for direct measurement of aerosol pH.

chemical components.[31,39] Both the phase partitioning method and thermodynamic models are sensitive to input measurement values and their associated uncertainties, which can be high for species such as ammonia. Also, both assume gas–particle equilibrium, which is not always accurate, especially as aerosols are often in nonideal states due to low liquid water content and high ionic strength.[31,40] Additionally, neither method accounts for most organic components, which are ubiquitous in the atmosphere.[41] This is a limitation as organic acids can influence acidity levels.[31,42] It should be noted that a few thermodynamic models make accommodations for organic species, such as a small number of dicarboxylic acids that can be incorporated into E-AIM calculations or a wider selection of organic compounds/functional groups available within AIOMFAC (aerosol inorganic–organic mixtures functional groups activity coefficients).[43] Direct measurement of aerosol pH is needed to provide an analytical determination of pH to constrain both model and proxy methods, particularly when the available methods disagree.

Currently, direct measurement of aerosol acidity is limited. One method uses colorimetric analysis integrated with a reflectance UV–Vis spectrometer to measure the proton mass concentration of particle samples collected on dyed filters.[44,45] While this technique does not rely on solvent extraction, it is an offline method that infers pH from an estimate of proton mass based on a correlation with the measured absorbance of the pH-sensitive dye.[44,45] Another method uses Raman microspectroscopy to quantify concentrations from the vibrational modes of an acid and its conjugate base to determine their equilibrium.[46,47] The concentrations are then combined with activity coefficient calculations to determine pH of individual particles.[46,47] Application of this method has been limited though, as it has only been used to measure pH for laboratory-generated supermicrometer particles composed of simple chemical compositions.[46,47]

Herein, we developed and applied a facile method for direct, quantitative, real-time measurement of size-resolved ensemble average (bulk) aerosol pH (molality-based). This method uses pH indicator paper to colorimetrically determine aerosol acidity, thus eliminating the dependence on challenging particle composition measurements or isolation of specific acid/conjugate base species for direct pH measurement via Raman spectroscopy.[47] While a limited number of studies have measured cloud and fog droplet acidity qualitatively with pH indicator paper method previously,[48,49] this has not been explored quantitatively. Aerosol samples were collected on pH indicator paper using a multiple stage impactor, allowing size-resolved aerosol acidity to be measured. In this work, size-dependent trends in aerosol acidity were observed for $(NH_4)_2SO_4$–$H_2SO_4$ aerosol particles, with smaller particles being more acidic. This trend was confirmed with single-particle pH measurements via the previously discussed spectroscopic method.[46,47] Lastly, preliminary ambient atmospheric measurements with pH indicator paper are presented to demonstrate the field capabilities of this method.

## METHODS

Standard solutions were prepared using 18.3 MΩ Milli-Q water and the following chemicals: ammonium sulfate $(NH_4)_2SO_4$ (Alfa Aesar) and sulfuric acid ($H_2SO_4$) (Sigma-Aldrich). All chemicals were >98.0% purity and used without further purification. Solutions were 30 mM $(NH_4)_2SO_4$ with varying concentrations of $H_2SO_4$ to control pH. Bulk solution pH values ranged from 0 to 4.5, as measured by a pH probe (AP110, accumet Portable). Aerosols were generated from solution using a Collison nebulizer operated with HEPA-filtered air, and then impacted onto pH indicator paper (MColorpHast pH test strips, Millipore Sigma) and quartz substrates (Ted Pella, Inc.) using a microanalysis particle sampler (MPS-3, California Measurements, Inc.). The MPS-3 consists of three stages with aerodynamic diameter ($d_a$) 50% size cuts of 2.5–5.0, 0.40–2.5, and <0.40 $\mu$m for stages 1, 2, and 3, respectively. The chemical composition of the aerosol particles was chosen based on the ubiquity of sulfate in submicrometer atmospheric particles, which results in it being a common seed for SOA chambers study experiments.[50] The pH range was chosen based on predictions of acidic aerosol particles from previous studies.[22−26,28] Aerosol particles were not dried prior to impaction to ensure they were aqueous, and the RH of the system was maintained at ∼90%.

Aerosol pH for aqueous particles collected from each stage of the MPS on pH indicator paper was determined by



DOI: 10.1021/acs.analchem.8b00586
Anal. Chem. 2018, 90, 11232−11239

colorimetric analysis of images collected immediately after sampling (Figure 1). pH indicator paper for the pH ranges of 0−2.5 and 2.5−4.5 were used for this study. For the pH 0−2.5 paper, the indicator dye is thymol blue with a p$K_a$ of 1.7, and for the pH 2.5−4.5 paper, the indicator dye is methyl orange with a p$K_a$ of 3.47. An image of each sample, the corresponding pH color scale, and a blank pH indicator strip was collected with a standard cellular phone camera. The Red, Green, and Blue channels of the pH color scale were analyzed with a custom MATLAB script written for this purpose to create a calibration curve relating the difference between the Green and Blue channels to pH[2]. The pH of the sample was then determined using the calibration curve. The pH color scale is included in each picture to generate a calibration curve for each sample analyzed to account for differences between images. Uncertainty for each pH measurement is also calculated based on color variation within the sample. pH indicator paper measurements of bulk solution standards of $(NH_4)_2SO_4$−$H_2SO_4$ of varying pH were compared to pH probe measurements to confirm the accuracy of the pH indicator paper and image processing method (Figure S1). A correction factor was applied to all measurements made with the higher range pH paper due to a small, systematic bias with the pH 2.5−4.5 indicator paper, and further information is provided in the Supporting Information (Figure S2). To confirm the color change on the pH indicator paper was due to aerosol particles rather than gas or water vapor, a blank in which the particles were filtered out using a HEPA filter was collected, and there was no observed color change on the pH indicator paper (Figure S3). To account for potential differences in measured pH between calibration reference solutions and inorganic ions common in atmospheric aerosols, a range of aqueous inorganic solutions were tested with both pH probe and pH indicator paper (Figure S4).

For comparison to the bulk aerosol pH from the pH indicator paper, the pH of individual particles was also determined using the Raman microspectroscopic method described by Rindelaub et al.[46] and Craig et al.[47] pH is ultimately determined based on molality according to eq 1.[46,47,51] Details on the Raman analysis are provided in the Supporting Information.

$$\mathrm{pH} = -\log(a_{H^+}) = -\log(\gamma_{H^+}[H^+]) \quad (1)$$

Generated particles for each solution were also characterized by a scanning mobility particle sizer (SMPS, model 3938, TSI Inc.) and aerodynamic particle sizer (APS, model 3321, TSI Inc.). The SMPS was operated at a 10:1 sheath/aerosol flow ratio and provided mobility diameter ($d_m$) number and mass concentrations for the size range of 14.1−763.5 nm. The APS provided aerodynamic diameter ($d_a$) number and mass concentrations for the size range of 0.542−19.81 $\mu$m. Aerosols were studied under high (∼90%) and low (∼45%) RH conditions in order to determine the water content fraction for particles at 90% RH. For the low RH condition, aerosols passed through two diffusion dryers prior to analysis. RH was monitored with an RH sensor (EK-H5, Sensiron).

Raman spectra for individual impacted particles were collected using a LabRAM HR Evolution Raman microspectrometer (Horiba, Ltd.) equipped with a Nd:YAG laser source (50 mW, 532 nm) and CCD detector and coupled with a confocal optical microscope (100× 0.9 N.A. SLMPlan N Olympus objective).[52] The instrument was calibrated against the Stokes Raman signal of pure Si at 520 cm$^{-1}$ using a silicon wafer standard. Spectra from 500 to 1400 cm$^{-1}$ were acquired for 15 s with three accumulations. A 600 groove/mm diffraction grating yielded spectral resolution of ∼1.7 cm$^{-1}$. Although particles were generated and impacted at 90% RH, spectra were collected at ambient temperature and RH (∼35% or ∼60%). Though the aerodynamic diameter for particles collected on the smallest stage (<0.4 $\mu$m) is below the typical detectable particle size due to the diffraction limit of visible light and the 532 nm laser for the 100× objective, aqueous particles spread when impacted, causing a larger projected area diameter, which can be observed with typical spreading ratios.[53]

Ambient aerosol samples were also collected for pH indicator paper measurements using the MPS-3 impactor.[54] Sampling was conducted at the University of Michigan Biological Station (UMBS) PROPHET Tower (Pellston, MI) in July 2016 and the University of Michigan Chemistry Building (Ann Arbor, MI) in August 2016.

## RESULTS AND DISCUSSION

Herein, the first direct, quantitative measurements of size-resolved aerosol pH were made using pH indicator paper. Aerosol particles were generated from $(NH_4)_2SO_4$−$H_2SO_4$ solutions (pH range of 0−4.5) and impacted onto the pH indicator paper using a cascade impactor with three stages. Changes in aerosol acidity as a function of particle size were primarily observed at acidities below the p$K_a$ of $HSO_4^-$ (1.99) (Figure 2).[55] For aerosols generated from solutions with pH < 2.5, the aerosol pH of the coarse-mode particles ($d_a$ > 2.5 $\mu$m) was similar to that of the bulk solutions. In contrast, below a pH of 2.5, fine-mode aerosol ($d_a$ 0.4−2.5 $\mu$m) pH was lower than those of the bulk solution and coarse-mode particles. Aerosol pH of the smallest-sized particles ($d_a$ < 0.4 $\mu$m) was even lower, indicating particle acidity increases (pH decreases) with decreasing particle size. It should be noted that the minimum pH value calculated with the pH indicator paper method is pH 0 (the lowest value on the pH scale range for the pH 0−2.5 indicator paper), and thus represents an upper bound of pH for samples generated from solutions with pH ≤ 1. The increasing acidity of smaller particles is likely related to aerosol water content and ammonia partitioning below the p$K_a$ of bisulfate and is discussed in detail below.

Raman spectra collected from aerosol particles of various sizes corresponding to the pH paper measurement size ranges confirmed the observation of increased particle acidity with decreasing particle size (Figure 2, parts B and C). As shown in Rindelaub et al.[46] and Craig et al.,[47] the $\nu_s(SO_4^{2-})$ and $\nu_s(HSO_4^-)$ vibrational modes can be used to determine aerosol particle pH based on the $HSO_4^-/SO_4^{2-}$ acid−base equilibrium. For spectra normalized to the intensity of the $\nu(HSO_4^-)$ mode, a clear decrease in the intensity of the $\nu(SO_4^{2-})$ mode, indicating increasing acidity (decreasing pH), is observed with decreasing particle size across all bulk solution pH systems. Raman spectra for the other systems between pH 0.15 and 2.05, the pH range for which aerosol particle pH can be determined spectroscopically for the $HSO_4^-/SO_4^{2-}$ equilibrium,[47] is provided in the Supporting Information (Figure S5).

To further investigate the relationship between particle size and acidity, individual aerosol particle pH was determined spectroscopically for particles generated from bulk solution of pH 0.15 to pH 2.05. As shown in Figure 3, the single-particle spectroscopic pH measurements corroborate the aerosol pH


DOI: 10.1021/acs.analchem.8b00586
Anal. Chem. 2018, 90, 11232−11239

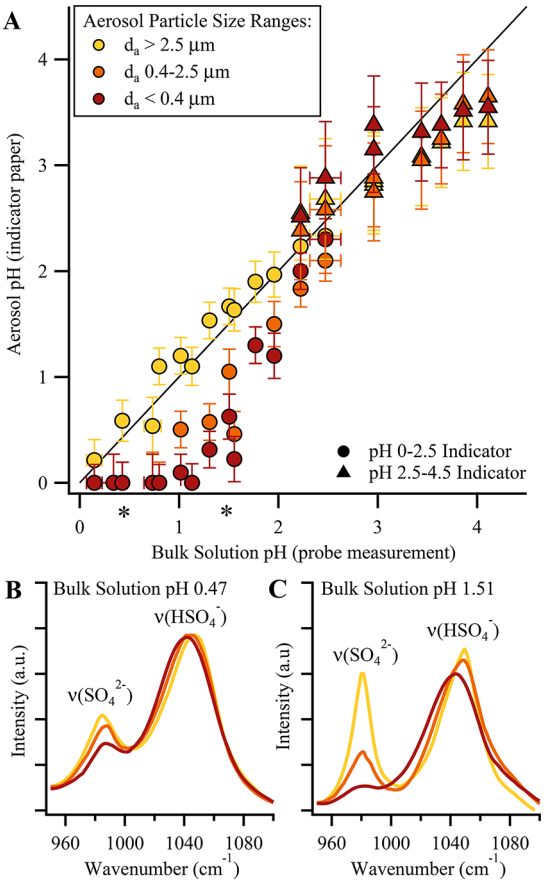


**Figure 2.** (A) pH indicator paper measurements of aerosol particles $d_a$ > 2.5 $\mu$m (yellow), $d_a$ 0.4−2.5 $\mu$m (orange), and $d_a$ < 0.4 $\mu$m (red) as a function of the bulk solution pH from which the particles were generated. Raman spectra of the $\nu(SO_4^{2-})$ and $\nu(HSO_4^-)$ modes, normalized to the $\nu(HSO_4^-)$ mode, for particles generated from bulk solution (B) pH 0.47 and (C) pH 1.51 (corresponding data marked by the *).

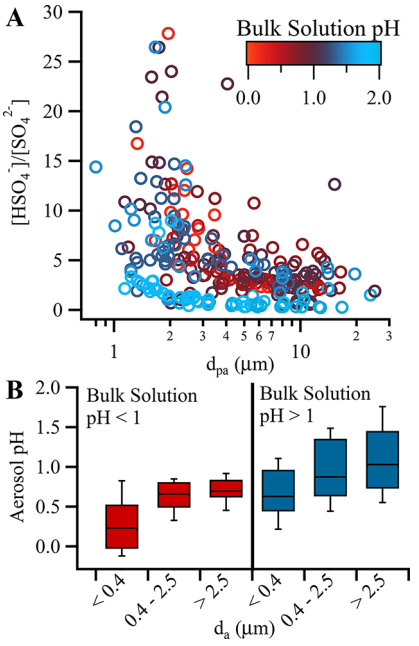


**Figure 3.** (A) $[HSO_4^-]/[SO_4^{2-}]$ as a function of $d_{pa}$ for individual aerosol particles, with color representing the pH of the solution from which the particles were generated. (B) Box and whisker plot of aerosol pH as a function of $d_a$ for individual particles, but grouped into size ranges corresponding to the pH indicator paper measurements. The centerline represents the median, the box outlines the inner quartiles, and the whiskers represent the 10th and 90th percentile.

indicator paper measurements. Particles generated from bulk solutions of lower pH had higher acidity levels, as expected, and across all bulk solution pH systems, the $[HSO_4^-]/[SO_4^{2-}]$ ratio is higher and more varied for smaller-sized particles, indicating higher levels of acidity and decreased uniformity within the aerosol population. When clustered according to the size ranges corresponding to the pH indicator paper measurements, increasing acidity with decreasing particle size can be clearly seen for systems both pH < 1 and pH > 1. As the pH indicator paper particle size ranges from inertial separation are based on aerodynamic diameter ($d_a$) rather than projected area diameter ($d_{pa}$),[56] the measured $d_{pa}$ of the individual particles analyzed by Raman was converted to $d_a$ prior to clustering based on a spreading ratio of 4.[53,57] For bulk solution systems pH < 1, particles with aerodynamic diameter < 0.4, 0.4−2.5, and > 2.5 $\mu$m had median pH values of 0.23, 0.66, and 0.69, respectively. For bulk solution systems pH > 1, particles with aerodynamic diameter < 0.4, 0.4−2.5, and > 2.5 $\mu$m had median pH values of 0.63, 0.87, and 1.03, respectively. Considering the log scale of $[H^+]$ for pH, these differences of ∼0.5 pH units correspond to a 3× increase in $H^+$ concentration as particle size decreases from supermicrometer to submicrometer for aerosol particles of the same population.

The observed trend of increasing particle acidity with decreasing particle size for systems where pH < 2.5 is attributed to ammonia partitioning and water loss. Below the $pK_a$ of bisulfate, loss of $NH_4^+(aq)$ to $NH_3(g)$ partitioning leaves less $NH_4^+(aq)$ present in the particle phase to neutralize sulfate species (eq 2). Although the smallest particle size range classified is < 0.4 $\mu$m, the example number concentration size distribution provided in the Supporting Information (Figure S6) shows that particles < 0.1 $\mu$m where $NH_3(g)$ volatilization would most likely occur are present. Though direct measurements of $NH_3(g)$ and quantified $NH_4^+(aq)$ were not available, this equilibrium likely plays a role and will be explored in future work.

$$SO_4^{2-}(aq) + NH_4^+(aq) \rightarrow HSO_4^-(aq) + NH_3(g) \quad (2)$$

Increased surface-area-to-volume ratios for smaller particles compared to larger particles allows for greater loss of water and potential $NH_3$ diffusion and partitioning from the particle to gas phase. With a lower water content, the molar concentration of chemical species (e.g., $[H^+]$) increases. Thus, in smaller-sized particles $[H^+]$ increases and pH decreases. Water content fraction by mass for each size range of particles for several pH systems was calculated based on comparison of mass concentration size distributions at wet and dry RH conditions. More details on the water content fraction calculation are provided in the Supporting Information. Increasing water content fraction was observed with increasing pH, as well as with increasing particle size, across all pH levels (Table S1). Particle density, calculated as part of the Raman spectroscopic method to determine pH,[46,47] corroborated the water content fraction results, as particle density increased with decreasing particle size (Table S1). These observations of water content fraction and particle density support the hypothesis that smaller particles contain less water and have higher


DOI: 10.1021/acs.analchem.8b00586
Anal. Chem. 2018, 90, 11232−11239

concentrations of chemical species, leading to lower measured pH values. Both loss of $NH_4^+(aq)$ due to $NH_3(g)$ partitioning and water loss lead to solutions that are no longer thermodynamically ideal water droplets with higher ionic strengths and higher levels of acidity.

This trend of increasing particle acidity with decreasing particle size has been indirectly observed for ambient aerosol previously.[16,48,58−60] The pH of coarse-mode aerosol was reported to be higher than that of fine-mode aerosol for several different particle types, including sea salt aerosol particles,[58] fog and cloud droplets,[48] and urban particles.[16,59,60] For these observations, aerosol pH was determined via extrapolation of pH measurements of diluted samples,[58] ion balance,[60] thermodynamic modeling,[16,59] or a qualitative pH paper method.[48] Several hypotheses were proposed to explain the observed differences in acidity, including differing rates of HCl volatilization,[58] dilution by condensation,[48] differing rates of neutralization,[60] and size-dependent neutralization by mineral cations[16] or gas-phase $NH_3$.[59] Given the complex nature of aerosol particles in terms of chemical composition and atmospheric conditions, it is likely that there are many factors that influence aerosol acidity with regards to particle size, and further studies are needed to elucidate the potential mechanisms driving this phenomenon.

Direct comparison of aerosol pH from pH indicator paper and single-particle pH from Raman microspectroscopy is presented in Figure 4. The Raman measurements represent the average pH for individual particles analyzed within each size range (converted from $d_{pa}$ to $d_a$), with error bars indicating standard deviation. There is good agreement between the two methods across all size ranges. The largest deviation between the two methods is observed for particles generated from solution pH < 1.5 for the $d_a$ 0.4−2.5 $\mu$m size range, with the Raman spectroscopically determined pH values ∼0.5 pH units higher than the pH indicator paper determined pH values. This is most likely due to a limitation of the Raman spectroscopic method, as when one of the species in the bisulfate−sulfate equilibrium is more dominant, it is more difficult to accurately measure both vibrational modes. It should also be noted that the pH values plateau at ∼pH 0 for particle size ranges $d_a$ < 0.4 $\mu$m and 0.4−2.5 $\mu$m because both methods have a lower limit of pH 0. A comparison of pH indicator paper and Raman microspectroscopic aerosol pH measurements to model-predicted aerosol pH is included in the Supporting Information.

To investigate the detection limit of the pH indicator paper method, the minimum mass of particles needed to induce a quantifiable color change on the indicator paper for each size range was determined (Figure 5). The mass of particles impacted for each size range was calculated by integrating the area under the curve for mass concentration size distributions collected via SMPS and APS. The minimum mass required was determined by decreasing sampling time until a color change on the pH indicator paper was no longer distinguishable optically, both visually and by the image processing script. RH, and consequently, aerosol liquid water content, plays an important role in how much particulate mass is required, as water is needed for the dye in the indicator paper to change and diffuse throughout the paper enough to be visible. For $(NH_4)_2SO_4$−$H_2SO_4$ particles for most size ranges and pH conditions at RH 90%, on average based on these measurements, ∼65 $\mu$g of aerosol mass is sufficient for an accurate aerosol pH measurement. As particle pH increases, the necessary mass of particles also increases, since $[H^+]$ becomes more dilute. The smaller particle sizes of the lowest pH system (pH 0.15) are the exception to this trend, most likely due to

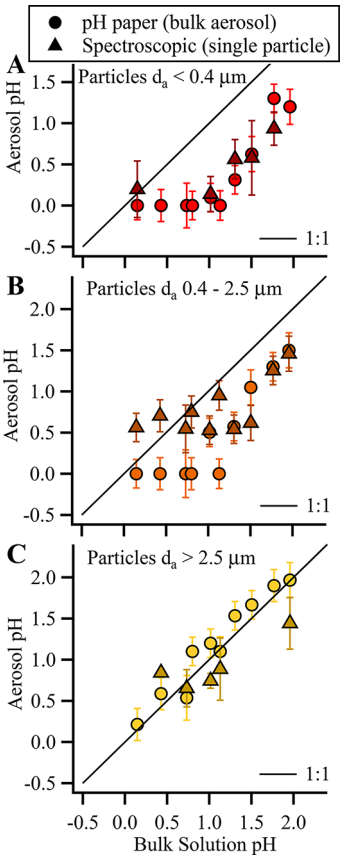


**Figure 4.** Aerosol pH as a function of the pH of the bulk solution from which the particles were generated to compare pH indicator paper and Raman spectroscopic methods for measuring aerosol pH for particles: (A) $d_a$ < 0.4 $\mu$m, (B) $d_a$ 0.4−2.5 $\mu$m, and (C) $d_a$ > 2.5 $\mu$m. Error bars for the pH indicator paper data corresponds to uncertainty in the measurements across multiple trials. Error bars for the Raman spectroscopic data corresponds to standard deviation of multiple trials.

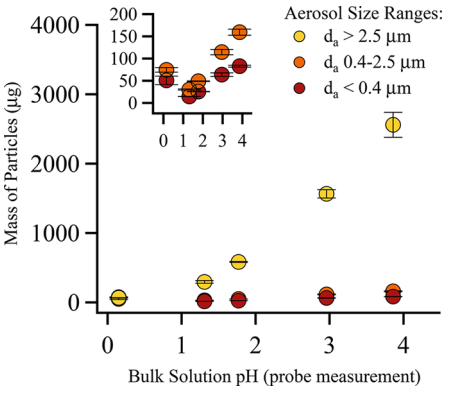


**Figure 5.** Minimum mass of particles needed to induce a measurable color change on the pH indicator paper for each particle size range for particles generated from solutions of varying pH. Error bars represent uncertainty in the calculation of the mass of particles based on multiple measurements of the mass concentration size distribution. Note: the error bars are difficult to see on this scale, so black error bars were used. Inset focuses on smaller mass range for $d_a$ 0.4−2.5 and <0.4 $\mu$m particles.



DOI: 10.1021/acs.analchem.8b00586
Anal. Chem. 2018, 90, 11232−11239

lower water content fraction (Table S1), which requires a larger mass of particles for sufficient liquid water to induce a color change on the pH indicator paper. Concurrently, the larger-sized particle range requires significantly more particulate mass, as both the mass and water content fraction of the larger particles are much greater than for those of the smaller-sized particles. Specific mass values are provided in Table S1. It should be noted that, under lower RH conditions, it is likely that greater particle mass will be necessary for pH indicator paper measurements, as the aerosol liquid water content will be lower. Future work will thoroughly investigate the limitations with respect to aerosol water content and RH for the pH indicator paper method of measuring aerosol pH.

To demonstrate the potential for ambient sampling with this method, as well as to illustrate some potential challenges, ambient aerosol particle samples were collected at two locations—the UMBS near Pellston, MI and outside the University of Michigan Chemistry Building in Ann Arbor, MI, as shown in Figure 6. As discussed in the Methods section, the

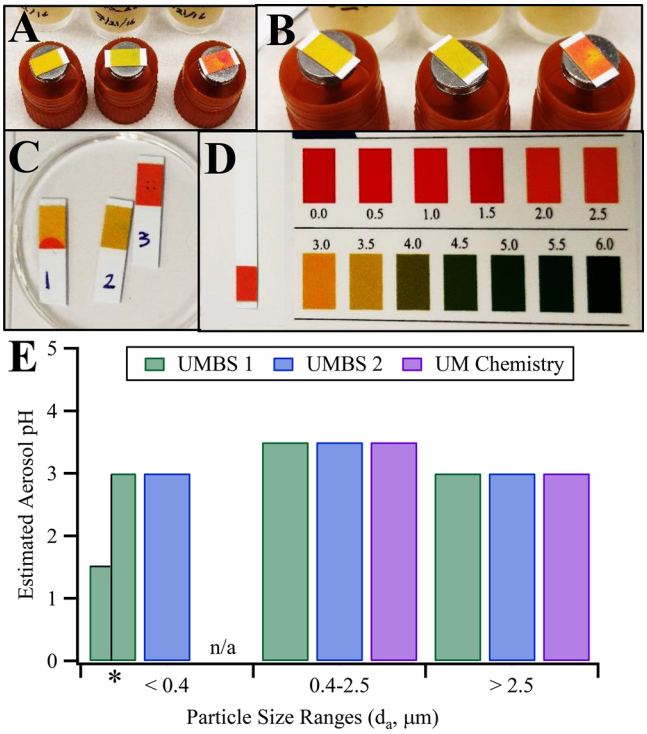


**Figure 6.** Images of ambient aerosol collected on pH indicator paper UMBS (A and B) and UM Chemistry building (C) with the pH indicator paper scale and blank (D). (E) Estimated aerosol pH based on comparison of the images to the color scale for each ambient sample. Note: two color changes corresponding to pH 1.5 and pH 3 were observed for the UMBS 1 < 0.4 $\mu$m sample, although pH 3 was more predominant, and a color change was not observed on the paper for the UM Chemistry < 0.4 $\mu$m sample.

pH of solutions of varying inorganic ion composition was successfully measured with pH indicator paper, thus indicating this method could also be applied to measure the pH of ambient aerosol particles of varying chemical composition. Ambient RH was ~70%, 80%, and 60% at the time of sampling for the UMBS 1, UMBS 2, and UM Chemistry samples, respectively. Ambient samples were collected for ~1−2 h, demonstrating that the pH indicator paper method can be run rapidly enough for semicontinuous measurements. For samples from both locations, aerosol acidity was primarily estimated to be ~pH 3.0−3.5 across the particle sizes measured. One sample from UMBS (Figure 6A) indicated that the smallest particles were more acidic (pH ~ 1.5), though the color change was not uniform across the samples and other portions of the paper had pH close to 3. pH could only be qualitatively determined from visual inspection for these samples, as the pH indicator paper used for sampling was not compatible with the MATLAB script for more quantitative analysis. However, the ambient aerosol pH measurements agree with the pH measurements of the laboratory-generated particles of this study, as aerosol particles with lower acidity levels (~pH 3−3.5) showed minimal difference in measured pH with regards to particle size. While the images of these ambient samples show they primarily contained nonaborbsing (e.g. no color) chemical species, the large area of the pH indicator paper that changed color around the center where aerosol particles were impacted shows the potential for pH analysis of ambient samples that may have slight discoloration at the impaction center from chemical species absorbing in the visible, such as black carbon and dust. These preliminary results demonstrate the potential for ambient measurement; however, it should be noted that further testing with precisely controlled RH and aerosol water content are needed to utilize the pH indicator paper method quantitatively for ambient studies.

## CONCLUSIONS

This study presents a facile method for direct measurement of aerosol pH through quantitative colorimetric analysis of aqueous aerosol samples. $(NH_4)_2SO_4$−$H_2SO_4$ aerosol particles of varying pH were generated and collected on pH indicator paper with a three-stage impactor with aerodynamic size cuts of $d_a$ < 0.4, $d_a$ 0.4−2.5, and $d_a$ > 2.5 $\mu$m, enabling analysis of size-resolved aerosol pH. For systems pH < 2, aerosol acidity increased with decreasing particle size, due to ammonia partitioning below the p$K_a$ (1.99) of bisulfate and loss of water as surface-area-to-volume ratios increased. Comparison with direct measurement of individual aerosol particle pH via a previously established spectroscopic method corroborated these results. The limit of detection for the pH indicator method in terms of particulate mass necessary for a measurable color change shows that, on average, ~65 $\mu$g of particulate mass was needed for fine particles (<2.5 $\mu$m), while the mass for more dilute, larger particles increased with pH, requiring total particulate masses of ~65 $\mu$g at pH 0 and ~2.5 mg at pH 4. Preliminary ambient measurements with sampling times of ~1−2 h demonstrate the potential for atmospheric application of this method. Further work investigating the effect of RH and aerosol liquid water content is needed to make ambient sampling robust. Future studies of aerosol acidity enabled by this method of direct, real-time measurement of aerosol pH have the potential to constrain ambient aerosol acidity experimentally. This is needed as key processes, such as SOA formation in the southeastern United States and nitrate haze events in Beijing, are strongly dependent on aerosol acidity, but pH values have thus far been determined indirectly and without measurement validation.[22,61] Additionally, aerosol pH can be highly dynamic, particularly for aerosols initially emitted in an alkaline state (sea spray aerosol and lake spray aerosol).[58,62,63] Fundamental studies of aerosol acidity have the potential to improve understanding of pH-dependent multiphase chemical processes, which are needed to improve


DOI: 10.1021/acs.analchem.8b00586
Anal. Chem. 2018, 90, 11232−11239

the predictive capability of atmospheric models focused on human health and climate.

## ■ ASSOCIATED CONTENT

### Supporting Information

The Supporting Information is available free of charge on the ACS Publications website at DOI: 10.1021/acs.analchem.8b00586.

pH indicator paper measurements of bulk solution standards of $(NH_4)_2SO_4$−$H_2SO_4$ and HCl, images of aerosol blank testing, pH indicator paper measurement of solutions of varying inorganic composition, Raman spectra of particles of various sizes under different of pH conditions, information on water content fraction and particle mass limit calculations and their respective values, information on E-AIM and ISORROPIA-II modeling, and a comparison of measured and model-predicted aerosol pH (PDF)

## ■ AUTHOR INFORMATION


### Corresponding Author

*E-mail: aulta@umich.edu.

### ORCID

Peter K. Peterson: 0000-0002-9337-6677
Lucy Nandy: 0000-0001-7647-9837
Cari S. Dutcher: 0000-0003-4325-9197
Andrew P. Ault: 0000-0002-7313-8559


### Notes

The authors declare no competing financial interest.

## ■ ACKNOWLEDGMENTS

This work was supported by National Science Foundation (NSF) Grants CHE-1654149 (CAREER, A.P.A.) and AGS-1554936 (CAREER, C.S.D.) and University of Michigan (UM) startup funds. R.L.C. was partially supported by the Susan Lipschutz Fellowship Award. R.D.C. was supported by a Rackham Merit Fellowship Award and the Marian P. and David M. Gates UMBS Graduate Student Fellowship. S.C. and M.A.H. were supported by the Detroit Research Internship Summer Experience (D-RISE) program, by NSF Grants CHE-1654149 (A.P.A.) and CHE-1305777 (Dr. Nicolai Lehnert), other UM sources, and Cass Technical High School. Dr. Simon Clegg is thanked for helpful discussions.

## ■ REFERENCES


(1) Kim, K.-H.; Kabir, E.; Kabir, S. *Environ. Int.* **2015**, *74*, 136−143.
(2) Pöschl, U. *Angew. Chem., Int. Ed.* **2005**, *44*, 7520−7540.
(3) Jang, M.; Czoschke, N. M.; Lee, S.; Kamens, R. M. *Science* **2002**, *298*, 814−817.
(4) Gaston, C. J.; Riedel, T. P.; Zhang, Z.; Gold, A.; Surratt, J. D.; Thornton, J. A. *Environ. Sci. Technol.* **2014**, *48*, 11178−11186.
(5) Lin, Y.-H.; Zhang, Z.; Docherty, K. S.; Zhang, H.; Budisulistiorini, S. H.; Rubitschun, C. L.; Shaw, S. L.; Knipping, E. M.; Edgerton, E. S.; Kleindienst, T. E.; Gold, A.; Surratt, J. D. *Environ. Sci. Technol.* **2012**, *46*, 250−258.
(6) Fitzgerald, E.; Ault, A. P.; Zauscher, M. D.; Mayol-Bracero, O. L.; Prather, K. A. *Atmos. Environ.* **2015**, *115*, 19−25.
(7) Ault, A. P.; Guasco, T. L.; Baltrusaitis, J.; Ryder, O. S.; Trueblood, J. V.; Collins, D. B.; Ruppel, M. J.; Cuadra-Rodriguez, L. A.; Prather, K. A.; Grassian, V. H. *J. Phys. Chem. Lett.* **2014**, *5*, 2493−2500.
(8) Prenni, A. J.; DeMott, P. J.; Kreidenweis, S. M. *Atmos. Environ.* **2003**, *37*, 4243−4251.
(9) Ghorai, S.; Laskin, A.; Tivanski, A. V. *J. Phys. Chem. A* **2011**, *115*, 4373−4380.
(10) Hu, K. S.; Darer, A. I.; Elrod, M. J. *Atmos. Chem. Phys.* **2011**, *11*, 8307−8320.
(11) Rindelaub, J. D.; McAvey, K. M.; Shepson, P. B. *Atmos. Environ.* **2015**, *100*, 193−201.
(12) Bondy, A. L.; Craig, R. L.; Zhang, Z.; Gold, A.; Surratt, J. D.; Ault, A. P. *J. Phys. Chem. A* **2018**, *122*, 303−315.
(13) Losey, D. J.; Parker, R. G.; Freedman, M. A. *J. Phys. Chem. Lett.* **2016**, *7*, 3861−3865.
(14) You, Y.; Smith, M. L.; Song, M.; Martin, S. T.; Bertram, A. K. *Int. Rev. Phys. Chem.* **2014**, *33*, 43−77.
(15) Ault, A. P.; Guasco, T. L.; Ryder, O. S.; Baltrusaitis, J.; Cuadra-Rodriguez, L. A.; Collins, D. B.; Ruppel, M. J.; Bertram, T. H.; Prather, K. A.; Grassian, V. H. *J. Am. Chem. Soc.* **2013**, *135*, 14528−14531.
(16) Fang, T.; Guo, H.; Zeng, L.; Verma, V.; Nenes, A.; Weber, R. J. *Environ. Sci. Technol.* **2017**, *51*, 2611−2620.
(17) Longo, A. F.; Feng, Y.; Lai, B.; Landing, W. M.; Shelley, R. U.; Nenes, A.; Mihalopoulos, N.; Violaki, K.; Ingall, E. D. *Environ. Sci. Technol.* **2016**, *50*, 6912−6920.
(18) Chen, H.; Laskin, A.; Baltrusaitis, J.; Gorski, C. A.; Scherer, M. M.; Grassian, V. H. *Environ. Sci. Technol.* **2012**, *46*, 2112−2120.
(19) Ault, A. P.; Gaston, C. J.; Wang, Y.; Dominguez, G.; Thiemens, M. H.; Prather, K. A. *Environ. Sci. Technol.* **2010**, *44*, 1954−1961.
(20) Rapf, R. J.; Dooley, M. R.; Kappes, K.; Perkins, R. J.; Vaida, V. *J. Phys. Chem. A* **2017**, *121*, 8368−8379.
(21) Liu, M. J.; Wiegel, A. A.; Wilson, K. R.; Houle, F. A. *J. Phys. Chem. A* **2017**, *121*, 5856−5870.
(22) Weber, R. J.; Guo, H.; Russell, A. G.; Nenes, A. *Nat. Geosci.* **2016**, *9*, 282−285.
(23) Guo, H.; Sullivan, A. P.; Campuzano-Jost, P.; Schroder, J. C.; Lopez-Hilfiker, F. D.; Dibb, J. E.; Jimenez, J. L.; Thornton, J. A.; Brown, S. S.; Nenes, A.; Weber, R. J. *J. Geophys. Res. - Atmos.* **2016**, *121*, 10355−10376.
(24) Guo, H.; Xu, L.; Bougiatioti, A.; Cerully, K. M.; Capps, S. L.; Hite, J. R., Jr.; Carlton, A. G.; Lee, S. H.; Bergin, M. H.; Ng, N. L.; Nenes, A.; Weber, R. J. *Atmos. Chem. Phys.* **2015**, *15*, 5211−5228.
(25) Battaglia, M. A.; Douglas, S.; Hennigan, C. J. *Environ. Sci. Technol.* **2017**, *51*, 13095−13103.
(26) Liu, M.; Song, Y.; Zhou, T.; Xu, Z.; Yan, C.; Zheng, M.; Wu, Z.; Hu, M.; Wu, Y.; Zhu, T. *Geophys. Res. Lett.* **2017**, *44*, 5213−5221.
(27) Shi, G.; Xu, J.; Peng, X.; Xiao, Z.; Chen, K.; Tian, Y.; Guan, X.; Feng, Y.; Yu, H.; Nenes, A.; Russell, A. G. *Environ. Sci. Technol.* **2017**, *51*, 4289−4296.
(28) Bougiatioti, A.; Nikolaou, P.; Stavroulas, I.; Kouvarakis, G.; Weber, R.; Nenes, A.; Kanakidou, M.; Mihalopoulos, N. *Atmos. Chem. Phys.* **2016**, *16*, 4579−4591.
(29) Wu, X.; Deng, J.; Chen, J.; Hong, Y.; Xu, L.; Yin, L.; Du, W.; Hong, Z.; Dai, N.; Yuan, C.-S. *Aerosol Air Qual. Res.* **2017**, *17*, 2152−2164.
(30) Kumar, S.; Raman, R. S. *Atmos. Environ.* **2016**, *143*, 152−163.
(31) Hennigan, C. J.; Izumi, J.; Sullivan, A. P.; Weber, R. J.; Nenes, A. *Atmos. Chem. Phys.* **2015**, *15*, 2775−2790.
(32) Koutrakis, P.; Wolfson, J. M.; Spengler, J. D. *Atmos. Environ.* **1988**, *22*, 157−162.
(33) Kim, S. Y.; Sheppard, L.; Hannigan, M. P.; Dutton, S. J.; Peel, J. L.; Clark, M. L.; Vedal, S. J. *J. Exposure Sci. Environ. Epidemiol.* **2013**, *23*, 481−486.
(34) Clegg, S. L.; Brimblecombe, P.; Wexler, A. S. *J. Phys. Chem. A* **1998**, *102*, 2137−2154.
(35) Wexler, A. S.; Clegg, S. L. J. *J. Geophys. Res.* **2002**, *107* (D14), ACH14-1.
(36) Clegg, S. L.; Pitzer, K. S.; Brimblecombe, P. *J. Phys. Chem.* **1992**, *96*, 9470−9479.
(37) Fountoukis, C.; Nenes, A. *Atmos. Chem. Phys.* **2007**, *7*, 4639−4659.
(38) Nenes, A.; Pandis, S. N.; Pilinis, C. *Aquat. Geochem.* **1998**, *4*, 123−152.




DOI: 10.1021/acs.analchem.8b00586
*Anal. Chem.* 2018, 90, 11232−11239

(39) Murphy, J. G.; Gregoire, P. K.; Tevlin, A. G.; Wentworth, G. R.; Ellis, R. A.; Markovic, M. Z.; VandenBoer, T. C. *Faraday Discuss.* **2017**, *200*, 379−395.
(40) Shiraiwa, M.; Li, Y.; Tsimpidi, A. P.; Karydis, V. A.; Berkemeier, T.; Pandis, S. N.; Lelieveld, J.; Koop, T.; Poschl, U. *Nat. Commun.* **2017**, *8*, 15002.
(41) Kolb, C. E.; Worsnop, D. R. *Annu. Rev. Phys. Chem.* **2012**, *63*, 471−491.
(42) Silvern, R. F.; Jacob, D. J.; Kim, P. S.; Marais, E. A.; Turner, J. R.; Campuzano-Jost, P.; Jimenez, J. L. *Atmos. Chem. Phys.* **2017**, *17*, 5107−5118.
(43) Zuend, A.; Marcolli, C.; Luo, B. P.; Peter, T. *Atmos. Chem. Phys.* **2008**, *8*, 4559−4593.
(44) Jang, M.; Cao, G.; Paul, J. *Aerosol Sci. Technol.* **2008**, *42*, 409−420.
(45) Li, J.; Jang, M. *Aerosol Sci. Technol.* **2012**, *46*, 833−842.
(46) Rindelaub, J. D.; Craig, R. L.; Nandy, L.; Bondy, A. L.; Dutcher, C. S.; Shepson, P. B.; Ault, A. P. *J. Phys. Chem. A* **2016**, *120*, 911−917.
(47) Craig, R. L.; Nandy, L.; Axson, J. L.; Dutcher, C. S.; Ault, A. P. *J. Phys. Chem. A* **2017**, *121*, 5690−5699.
(48) Ganor, E.; Levin, Z.; Pardess, D. *Atmos. Environ., Part A* **1993**, *27*, 1821−1832.
(49) Ganor, E. *Atmos. Environ.* **1999**, *33*, 4235−4242.
(50) Riva, M.; Budisulistiorini, S. H.; Chen, Y.; Zhang, Z.; D'Ambro, E. L.; Zhang, X.; Gold, A.; Turpin, B. J.; Thornton, J. A.; Canagaratna, M. R.; Surratt, J. D. *Environ. Sci. Technol.* **2016**, *50*, 9889−9899.
(51) Buck, R. P.; Rondinini, S.; Covington, A. K.; Baucke, F. G. K.; Brett, C. M. A.; Camoes, M. F.; Milton, M. J. T.; Mussini, T.; Naumann, R.; Pratt, K. W.; Spitzer, P.; Wilson, G. S. *Pure Appl. Chem.* **2002**, *74*, 2169.
(52) Craig, R. L.; Bondy, A. L.; Ault, A. P. *Aerosol Sci. Technol.* **2017**, *51*, 1099−1112.
(53) Bondy, A. L.; Kirpes, R. M.; Merzel, R. L.; Pratt, K. A.; Banaszak Holl, M. M.; Ault, A. P. *Anal. Chem.* **2017**, *89*, 8594−8598.
(54) Craig, R. L.; Bondy, A. L.; Ault, A. P. *Anal. Chem.* **2015**, *87*, 7510−7514.
(55) Lide, D. R. *CRC Handbook of Chemistry and Physics: A Ready-Reference Book of Chemical and Physical Data*; CRC Press: Boca Raton, FL, 2009.
(56) Hinds, W. C. *Aerosol Technology: Properties, Behavior, and Measurement of Airborne Particles*, 2nd ed.; John Wiley & Sons: New York, 1999.
(57) Sobanska, S.; Falgayrac, G.; Rimetz-Planchon, J.; Perdrix, E.; Bremard, C.; Barbillat, J. *Microchem. J.* **2014**, *114*, 89−98.
(58) Keene, W. C.; Pszenny, A. A. P.; Maben, J. R.; Sander, R. *Geophys. Res. Lett.* **2002**, *29*, 5-1.
(59) Zhang, Q.; Jimenez, J. L.; Worsnop, D. R.; Canagaratna, M. *Environ. Sci. Technol.* **2007**, *41*, 3213−3219.
(60) Yao, X.; Ling, T. Y.; Fang, M.; Chan, C. K. *Atmos. Environ.* **2007**, *41*, 382−393.
(61) Wang, G.; Zhang, R.; Gomez, M. E.; Yang, L.; Zamora, M. L.; Hu, M.; Lin, Y.; Peng, J.; Guo, S.; Meng, J.; Li, J.; Cheng, C.; Hu, T.; Ren, Y.; Wang, Y.; Gao, J.; Cao, J.; An, Z.; Zhou, W.; Li, G.; Wang, J.; Tian, P.; Marrero-Ortiz, W.; Secrest, J.; Du, Z.; Zheng, J.; Shang, D.; Zeng, L.; Shao, M.; Wang, W.; Huang, Y.; Wang, Y.; Zhu, Y.; Li, Y.; Hu, J.; Pan, B.; Cai, L.; Cheng, Y.; Ji, Y.; Zhang, F.; Rosenfeld, D.; Liss, P. S.; Duce, R. A.; Kolb, C. E.; Molina, M. J. *Proc. Natl. Acad. Sci. U. S. A.* **2016**, *113*, 13630−13635.
(62) Axson, J. L.; May, N. W.; Colon-Bernal, I. D.; Pratt, K. A.; Ault, A. P. *Environ. Sci. Technol.* **2016**, *50*, 9835−9845.
(63) May, N. W.; Olson, N. E.; Panas, M. G.; Axson, J. L.; Tirella, P. S.; Kirpes, R. M.; Craig, R. L.; Gunsch, M. J.; China, S.; Laskin, A.; Ault, A. P.; Pratt, K. A. *Environ. Sci. Technol.* **2018**, *52*, 397−405.



DOI: 10.1021/acs.analchem.8b00586
*Anal. Chem.* 2018, 90, 11232−11239